# Twenty Crystal Structures of Bromodomain and PHD Finger Containing Protein 1 (BRPF1)/Ligand Complexes Reveal Conserved Binding Motifs and Rare Interactions

Jian Zhu and Amedeo Caflisch*

Department of Biochemistry, University of Zürich, Winterthurerstrasse 190, CH-8057 Zürich, Switzerland

Ⓢ *Supporting Information*

ABSTRACT: BRPF1 plays a scaffolding role in transcription. We report on fragment screening by high-throughput docking to the BRPF1 bromodomain which resulted in six chemotypes with very favorable ligand efficiency (0.45−0.50 kcal/mol per non-hydrogen atom). Twenty crystal structures of BRPF1/ligand complexes show structural conservation in the acetyllysine binding site, common binding motifs, and unusual interactions (e.g., the replacement of a conserved water molecule). The structural information is useful for the design of chemical probes.

BRPF1

Crystallography

Fragment docking
Hit rate = 38%

Fragments LE: 0.45 ~ 0.50
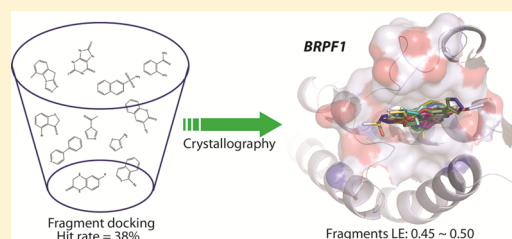
INTRODUCTION

Genetic analysis on zebrafish has shown that the bromodomain and PHD finger (BRPF) containing protein BRPF1 is a member of the Trithorax group with a central role during development in vertebrates.[1] BRPF1 associates with the histone acetyltransferase monocytic leukemia zinc finger protein (MOZ) and recruits it to distinct sites of chromatin. The bromodomain of BRPF1 binds to acetylated histone tails.[2]

In contrast to the bromodomain and extra terminal (BET) subfamily of bromodomains, e.g., bromodomain-containing protein 4 (BRD4), very few crystal structures of complexes of the BRPF1 bromodomain with ligands (holo) are available. Lubula et al.[3] reported the crystal structure of the BRPF1 bromodomain in complex with acetylated histone peptides H4K12ac and H2AK5ac. Demont et al.[4] identified 1,3-dimethyl benzimidazolones as potent BRPF1 bromodomain inhibitors and have disclosed the structures of two of these ligands in complex with BRPF1.

Experimental approaches to fragment-based screening have been used to identify ligands of bromodomains of the BET subfamily, viz., bromodomain-containing protein 2 (BRD2)[5] and BRD4,[6] and also for non-BET bromodomains, viz., ATPase family, AAA domain containing 2 (ATAD2),[7] bromodomain adjacent to zinc-finger domain 2B (BAZ2B),[8] and binding protein of the cAMP response element-binding protein (CREBBP).[9]

Here, we have screened a library of 24133 molecules by docking into the BRPF1 bromodomain followed by experimental validation of the in silico top ranking hits by X-ray crystallography. We could solve the crystal structures of BRPF1 (see Experimental Section for details) in the complex with 20 ligands at resolutions between 1.33 and 1.75 Å (Table 1). Six new chemotypes have been identified: tricyclazole, phenylpyridine, mercaptopurine, hydroxyisoquinoline, quinoxalin-2-one, and acetylindole. Common binding motifs and infrequent interactions emerge from the analysis of the 20 crystal structures. The acetyl lysine binding site of BRPF1 is conserved except for a slight displacement of the ZA loop. Only one of the 20 ligands displaces a conserved water molecule that is present in most crystal structures of bromodomain/ligand complexes.

RESULTS AND DISCUSSION

We screened in silico the 24133 molecules devoid of rotatable bonds and with molecular weight smaller than 550 g/mol (called fragments in the following) that were present in the 2014 version of the ZINC library.[13] The screening was carried out by high-throughput fragment docking into the structure of apo BRPF1 (PDB code 4LC2) using the program SEED[14] (see Experimental Section for details). Virtual screening required about 24 h; the preparation of the library of fragments took less than 1 h, and the docking of the 24133 fragments required less than a day on a commodity desktop. An initial set of 13 molecules among the top 30 ranking fragments was selected according to predicted binding energy (SEED energy) and availability and tested by experiments of soaking into crystals of the apo form of the BRPF1 bromodomain. The crystal structures of the complexes of BRPF1 with five of these fragments (**1**, **2**, **3**, **5**, and **8** in Table 1 and Supporting Information (SI), Figure S1) were solved. Electron densities were not observed for the other eight fragments (SI, Figure S2). The predicted binding mode of fragments **1**, **2**, and **8** was confirmed by the crystal structures (SI, Figure S1). Fragment **3** shows a different orientation in the crystal with respect to the docked pose, which is probably due to the lack of reorientation of the structural water molecules during docking. The oxygen atom of fragment **5** (1-isoquinolinone) replaces the buried water molecule that bridges to the side chain of the conserved Tyr665 (see below) and was present during docking. Thus, the

Table 1. Structures, K_D Values for BRPF1, and Ligand Efficiencies (LE) of in Silico Hits[a]
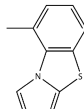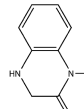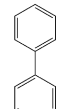
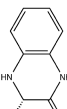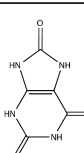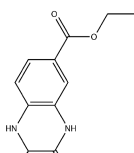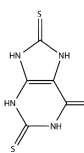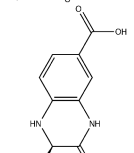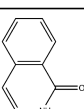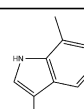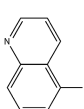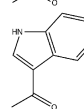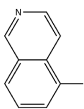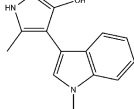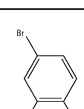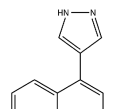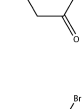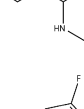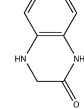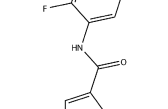| Cpd PDB ID	Structure	K_D (μM)	LE	Cpd PDB ID	Structure	K_D (μM)	LE
1 5EQ1		21	0.49	**11** 5EPS		38	0.50
2 5EWD		>200		**12** 5EPR		91	0.46
3 5E3G		>50		**13** 5EWC		N.D.	
4 5E3D		95	0.46	**14** 5DYA		>200	
5 5C87		>200		**15** 5ETB		29	0.48
6 5EM3		>200		**16** 5ETD		N.D.	
7 5EWH		170	0.47	**17** 5D7X		15	0.35
8 5C85		105	0.45	**18** 5EV9		N.D.	
9 5DYC		N.D.		**19** 5EVA		>200	
10 5DY7		>200		**20** 5C7N		0.27	0.32

Table 1. continued

[a]Molecules **1−16** can be clustered (SI, Figure S3) in six chemotypes (horizontal lines). The K_D values were determined by a competition binding assay BROMOscan[10] in duplicate (SI, Figure S4). For compound **20**, an IC$_{50}$ value of 0.65 μM was determined by AlphaScreen[11] (SI, Figure S5). Ligand efficiency[12] is calculated as LE = $(1.37/HA) \times pK_D$, in the units of kcal/mol per non-hydrogen atom.

hit rate, i.e., ratio of binders versus purchased fragments, is 38% (or 23% if one considers only the poses correctly predicted by docking).

An additional set of 15 molecules were tested in a second round of soaking experiments. This set consists of nine purchasable analogues (according to the definition in the ZINC database with a similarity threshold of 70%) of the five original hits, the acetylindole derivative **17** (which binds to another bromodomain of subfamily IV, the BRD9 bromodomain),[15] four molecules similar to **17** (compounds **15**, **16**, **18**, and **19**), and the pan-bromodomain inhibitor bromosporine (**20**).[16] In total, five ligands show a value of the equilibrium dissociation constant (K_D) for the BRPF1 bromodomain smaller than 100 μM while bromosporine has a K_D of 0.27 μM (Table 1). Importantly, the seven ligands with K_D < 200 μM (compounds **1**, **4**, **7**, **8**, **11**, **12**, and **15**) have very favorable ligand efficiency (LE) in the range 0.45−0.50 kcal/mol per non-hydrogen atom. Of these, fragments **1** and **8** are two of the five original docking hits.

For the analysis of the 20 crystal structures of the BRPF1 bromodomain/ligand complexes (Table 1), it is useful to describe first the binding site and common binding motifs. The acetyl lysine binding site has a parallelepiped-like shape in which the ligands are sandwiched by van der Waals contacts with the ZA-loop side chains Val657, Pro658, and Val662 on one of the two largest sides of the pocket and Ile652, Asn708, and Phe714 (the so-called gatekeeper) on the opposite side of the pocket (Figure 1). The bottom of the binding site is occupied by conserved water molecules and the phenyl ring of the conserved Phe653 (SI, Figures S6−S8). The structural overlap of the 20 complexes shows that the backbone and most side chains in the acetyl lysine binding site are conserved (Figure 1A). This finding is congruent with the similar size of the compounds, which consist of two or three (fused) ring systems. Furthermore, all crystals belong to the same space group and there are no crystal contacts in the acetyl lysine binding site. The structural similarity in the binding site is very high for the BC loop (residues 707−712) and the N-terminal segment of the ZA-loop (residues 650−656). The latter includes the Asn651-Ile652-Phe653 segment that corresponds to the Trp-Pro-Phe triad in the BET bromodomains. In contrast, the central segment of the ZA-loop (residues 657−668) shows structural heterogeneity. The rigid-body displacement of this part of the ZA-loop reduces the aperture of the binding site with respect to the apo structure (PDB code 4LC2), which was solved in the same space group as our 20 holo structures (Figure 1B). The slightly narrower binding pocket in the holo structures with respect to the apo conformation is a consequence of the intrinsic flexibility of the ZA-loop and the formation of optimal van der Waals contacts between the ligand and the hydrophobic side chains of Val657, Pro658, and Val662 on one side of the pocket and Ile652 and the gatekeeper Phe714 on the other side (Figure 1C). Quantitatively, the largest backbone displacement with
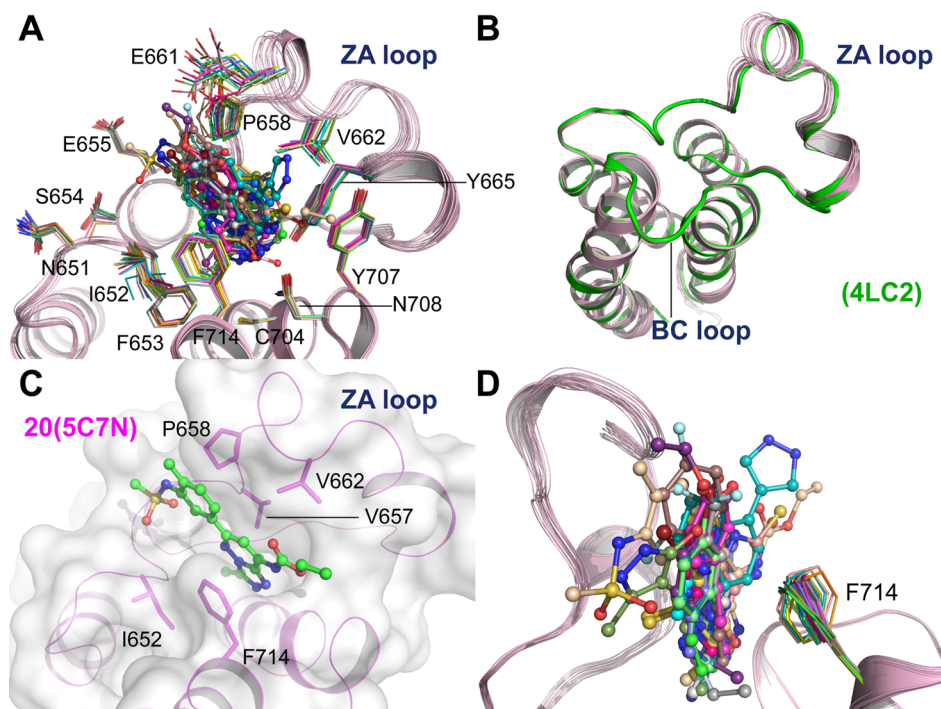
Figure 1. Structural overlap and analysis of the 20 complex structures. (A) Kac binding site of BRPF1. (B) Displacement of the ZA-loop in the 20 holo structures with respect to the apo structure (4LC2, green). (C) Hydrophobic residues lining the Kac binding site in BRPF1. (D) The phenyl ring of the gatekeeper residue Phe714 shows different orientations for different ligands.

respect to the apo structure is observed for the residues 659–661 whose Cα atoms move by up to 2.5 Å. The side chain of Glu661 shows the largest variability in the 20 structures (Figure 1A). Interestingly, the size of the ligand influences the orientation of the Glu661 side chain particularly for compounds **13**, **19**, and **20** (bromosporine), whose binding modes induce the largest displacement of the tip of the Glu661 side chain (SI, Figure S8). It is important to note that the slightly different tilting of the ligands is related not only to the rigid-body displacement of residues 657–668 of the ZA loop but also to the different orientations of the phenyl ring of the Phe714 gatekeeper (Figure 1D). The χ_2 dihedral angle of Phe714 varies in a range of about 75°, resulting in different orientations of the phenyl ring.

The two hydrogen bonds with the NH2 group of the conserved Asn708 and the buried water molecule that bridges to Tyr665 are present in all structures except for the complex with fragment **5** (Figure 2). In this complex, the oxygen atom of fragment **5** is at hydrogen bond distance to the hydroxyl oxygen of Tyr665 (2.7 Å) while its distance from the side chain nitrogen atom of Asn708 is 4.0 Å which is too long for a hydrogen bond. The scatter plot of the two hydrogen bond distances shows that the one with the structural water is shorter in 15 of 19 structures (Figure 3). This result is consistent with a previous study on BRD2 (ref 5) and provides further evidence that the hydrogen bond with the buried water molecule that bridges to the conserved Tyr665 is stronger than the one with Asn708.

The interaction with the carbonyl oxygen of the conserved Asn708 is heterogeneous. In the complexes with the ligands **9**, **10**, **12**, and **14**, there is a water molecule that acts as bridge to the side chain CO of Asn708 (Figure 4A,B). This water molecule corresponds to a structural water molecule of the apo structure (HOH1007 in 4LC2). In contrast, the bridging water
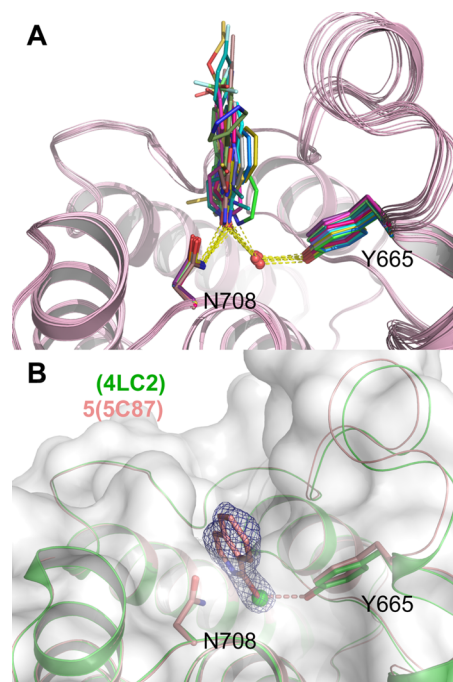
Figure 2. Only fragment **5** displaces the buried water molecule that acts as bridge to the conserved Tyr665. (A) Crystal structures overlay of all ligands but **5**. (B) Structural overlap of the complex with fragment **5** (pink) and the apo structure (green). $2F_o - F_c$ electron density map of **5** is shown in mesh contoured at 1 σ.

molecule is replaced by an NH group in ligands **3**, **4**, and **20** (Figure 4C) and the methyl group of compound **11** (Figure 4D). Similar to compound **11**, a previously reported 1, 3-dimethyl benzimidazolone inhibitor (SI, Figure S9) of the
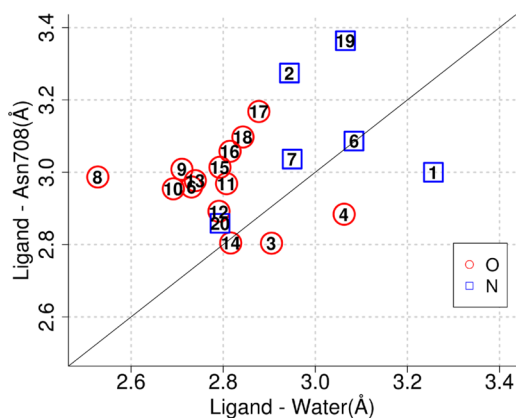
Figure 3. Scatter plot of hydrogen bond distances involving the ligand acceptor atom closest to the side chain N atom of the conserved Asn708. Numbers denote the ligand, and symbols the atomic element of the acceptor. In 15 of 19 structures, hydrogen bonds with the buried water that bridges to the Tyr665 side chain are shorter than with the Asn708.

BRPF1 bromodomain replaces the water molecule bridging to the side chain CO of Asn708 (PDB code 4UYE).

The molecules of the largest cluster (**8−14**) share the tetrahydroquinoxalin-2-one scaffold (Table 1). As mentioned above, these ligands do not form a direct hydrogen bond with the carbonyl oxygen of the Asn708 side chain (Figure 4, SI, Figures S7, S8). In contrast, in the structures of the complexes of the CREBBP bromodomain inhibitors[9] with the tetrahydroquinoxalin-2-one scaffold, there are two direct hydrogen bonds to the conserved asparagine (Asn1168 in CREBBP, PDB

codes 4NYW and 4NYX). The structural overlap shows that the position of the scaffold in the complexes with BRPF1 is slightly shifted with respect to CREBBP (SI, Figures S9, S10).

The two mercaptopurine fragments **3** and **4** show distinct binding mode as compared with a 2-amine-9*H*-purine derived BRD9 inhibitor[17] (SI, Figure S11). In both structures of **3** and **4**, the NH group at position 7 donates a hydrogen bond to the Asn708 side chain CO while the carbonyl group at position 6 forms a bifurcated hydrogen bond with the Asn708 side chain NH and the water molecule that bridges to Tyr665. In the BRD4 and BRD9 structures, the 2-amine-9*H*-purine derivative shows a flipped orientation with the amine group at position 2, nitrogen atom at 3, and NH group at 9 involved in hydrogen bonds to the conserved asparagine and water molecule.

Finally, a polar interaction with the backbone carbonyl of Ile652 is present in the complex with several ligands. This interaction was first observed in molecular dynamics simulations of the spontaneous binding of acetyl lysine.[18] In the complex structures with the quinoxalinone derivatives **8**, **9**, **10**, and **13**, there is a direct hydrogen bond with the carbonyl of Ile562, while a bridging water molecule is present for compounds **12**, **18**, and **19** (SI, Figures S7, S8).

■ CONCLUSIONS

We have identified six chemotypes of ligands of the BRPF1 bromodomain by high-throughput docking of fragments, which was carried out in 1 day on a single commodity processor, followed by soaking experiments and purchase of hit analogues. Seven in silico hits have ligand efficiency in the range 0.45−0.50 kcal/mol per non-hydrogen atom (Table 1). The X-ray crystal structures of BRPF1 in complex with 19 compounds (and the complex with bromosporine, a previously disclosed promiscu-
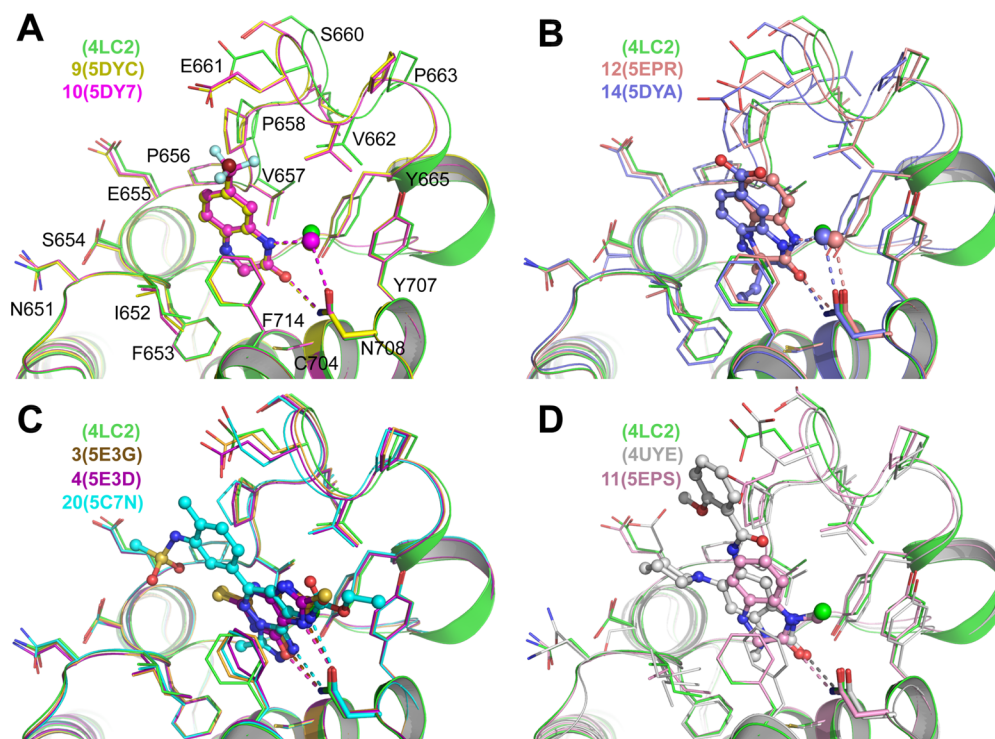
Figure 4. A water molecule acting as hydrogen bond bridge to the side chain carbonyl of Asn708 was observed in the crystal structures of the complexes with compounds (A) **9** and **10**, and (B) **12** and **14**. The bridging water molecule is replaced by the NH group of compounds **3**, **4** and **20** (C), and the methyl group of fragment **11** and a benzimidazolone derivative (4UYE) (D). The apo structure (4LC2, green) is shown in all panels as a basis of comparison.

ous inhibitor) show that the overall structure of the acetyl lysine binding site is conserved. Interestingly, the water-bridged hydrogen bond with the conserved tyrosine of the ZA-loop (Tyr665) is present in all crystal structures except for the complex with fragment **5** (1-isoquinolinone), whose oxygen atom replaces the buried water molecule which does not improve affinity. The phenyl ring of the gatekeeper residue (Phe714) shows slightly different orientations, while the ZA-loop accommodates different ligands by rigid-body displacement and rearrangement of side chains, in particular Glu661.

The fragment-based high-throughput docking campaigns in our group have resulted in the identification of molecules with very favorable ligand efficiency for the bromodomains of BRD4,[19] CREBBP,[20] BAZ2B,[21] and BRPF1 (this work). These bromodomains belong to four different subfamilies of human bromodomains (viz., subfamilies II, III, IV, and V). In the case of the CREBBP bromodomain, optimization of the initial hits by chemical synthesis of derivatives has generated several selective low nanomolar inhibitors with ligand efficiency similar to the initial hits.[20] Thus, the screening of fragment libraries by docking is very efficient and shows high success rate and negligible cost. The favorable ligand efficiency of our hits and their crystal structures in the complex with the BRPF1 bromodomain are important starting points for hit optimization and the design of chemical probes to investigate the function of BRPF1. For instance, the bromine-containing fragments **8** and **9** could be grown into more potent and selective ligands by Suzuki coupling.

■ EXPERIMENTAL SECTION

Fragment Docking. The nearly 12 million molecules of the ZINC database (version 2014)[13] were filtered for zero rotatable bonds and molecular weight smaller than 550 g/mol by the program DAIM.[22] The resulting library of 24133 fragments was docked into the apo structure of BRPF1 (PDB code 4LC2) by the program SEED,[14] which evaluates the binding energy using a force field-based energy function with a continuum dielectric approximation of desolvation penalties.[23] The binding site for docking was defined by the conserved asparagine in the BC loop (Asn708) and four buried water molecules (numbered w1 to w4 in SI, Figures S6–S8) which are present in most crystal structures of bromodomains. The partial charges and van der Waals parameters of the protein were taken from the CHARMM36 all-atom force field,[24] while the fragments were parametrized using the CHARMM general force field (CGenFF).[25] It is important to note that CGenFF is fully consistent with the CHARMM36 force field because they use the same paradigm for the derivation of partial charges, van der Waals parameters, and parameters for bonding interactions (covalent bonds, angles, dihedrals, and improper dihedrals). The value of the dielectric constant for the continuum calculations was set to 2.0 and 78.5 in the low-dielectric region (solute) and high-dielectric region (solvent), respectively. The docking of the 24133 fragments with SEED required nearly 22 h (about 3 s per fragment) of a single core of an i7-930 processor at 2.8 GHz.

Chemistry. All screened compounds were purchased from commercial vendors and the purity of all molecules was analyzed by HPLC-MS and is determined to be at least 95%. Compound **20** (bromosporine) was purchased from Sigma-Aldrich with purity higher than 98%.

Protein Production. The gene encoding the bromo-domain of BRPF1 (aa 626–740) was amplified by PCR from the original plasmid (Addgene plasmid no. 53620) and subcloned to a modified pGEX-4T-1 vector. A tobacco etch virus (TEV) protease recognition site was introduced between the glutathione S-transferase (GST) fusion protein and BRPF1 bromodomain. The recombinant plasmid was transformed into *Escherichia coli* strain BL21(DE3). The cells were grown at 37 °C until an OD600 of 0.6 was reached. After induction (0.2 mM IPTG) and overnight expression at 16 °C, the GST-tagged protein was purified by a Glutathione Sepharose 4B column and the GST tag was removed with TEV protease afterward. The bromodomain was further purified using a Superdex 75 column in the buffer of 50 mM HEPES (pH 7.5), 0.15 M NaCl, and 0.5 mM DTT. Eluted protein was concentrated to 22 mg/mL (NanoDrop spectrophotometer) in the same buffer and frozen in liquid nitrogen.

Crystallization. Sparse-matrix crystallization screens were performed with a Phoenix crystallization robot to identify initial crystallization conditions. BRPF1 bromodomain was crystallized by vapor diffusion in hanging drops at 4 °C. Crystallization buffer is composed of 0.1 M sodium acetate pH 5.5 (or 0.1 M BIS-TRIS propane pH 6.5), 0.15–0.2 M sodium nitrate, and 18–22% PEG3350. Overnight soaking of ligands was performed by transferring the apo crystals into the crystallization buffer in which the compounds were previously dissolved at 5 mM. Soaked crystals were cryoprotected with the crystallization buffer supplemented with 20% glycerol prior to freezing in liquid nitrogen. Fragments **5** and **6** were cocrystallized with BRPF1 in the crystallization buffer and cryoprotected the same way as the soaked crystals.

Data Collection and Structure Solution. Diffraction data were collected at the Swiss Light Source, Paul Scherrer Institute (Villigen, Switzerland), beamlines PXI and PXIII. Data were processed with XDS[26] and SCALA,[27] and structures were solved by molecular replacement with Phaser[28] using PDB 4LC2 as search model. Initial models were refined iteratively with Phenix[29] and manual model building with COOT.[30] Crystal data collection and refinement statistics are summarized in SI, Tables S1–S5.

BROMOscan and AlphaScreen Assays. BROMOscan technology is a competition experiment that uses an immobilized ligand and a DNA-tagged bromodomain protein.[10] Compounds that bind to the bromodomain of interest will prevent binding of the bromodomain to the immobilized ligand. The amount of captured bromodomain is quantified by qPCR, and the dissociation constants are calculated with a standard dose–response curve. Further details about the assays can be found in the SI. AlphaScreen assays[11] consist of a donor bead that is able to transfer singlet oxygen to an acceptor bead that is in the proximity, and as a result, the acceptor bead emits a luminescent/fluorescent signal. In the presence of a bromodomain ligand, the donor/acceptor complex is disrupted, leading to a loss of singlet oxygen transfer and loss of the fluorescent signal.

■ ASSOCIATED CONTENT

ⓢ Supporting Information

The Supporting Information is available free of charge on the ACS Publications website at DOI: 10.1021/acs.jmed-chem.6b00215.

> Molecular formula strings for ligands **1**–**20** (CSV)
>
> Experimental methods, X-ray crystal structure statistic data, and structural analyses of all reported crystal structures (PDF)

Accession Codes

PDB accession codes of the structures of the BRPF1 bromodomain in the complex with molecules **1**–**20** are **1** (5EQ1), **2** (5EWD), **3** (5E3G), **4** (5E3D), **5** (5C87), **6** (5EM3), **7** (5EWH), **8** (5C85), **9** (5DYC), **10** (5DY7), **11** (5EPS), **12** (5EPR), **13** (5EWC), **14** (5DYA), **15** (5ETB), **16** (5ETD), **17** (5D7X), **18** (5EV9), **19** (5EVA), and **20** (5C7N), respectively. Authors will release the atomic coordinates and experimental data upon article publication.

■ AUTHOR INFORMATION

Corresponding Author

*Phone: +41 44 635 55 21. Fax: +41 44 6356862. E-mail: caflisch@bioc.uzh.ch.

ABBREVIATIONS USED

Alpha, amplified luminescent proximity homogeneous assay; proteins ATPase family, AAA domain containing 2 (ATAD2); BAZ2B, bromodomain adjacent to zinc-finger domain 2B; BET, bromodomain and extra terminal; BRD2, bromodomain-containing protein 2; BRD4, bromodomain containing protein 4; BRD9, bromodomain containing protein 9; BRPF1, bromodomain and PHD finger (BRPF) containing protein 1; CREBBP, binding protein of the cAMP response element-binding protein; GST, glutathione S-transferase; Kac, N-ε-acetyl-lysine; MOZ, monocytic leukemia zinc finger protein; TEV, tobacco etch virus

REFERENCES

(1) Laue, K.; Daujat, S.; Crump, J. G.; Plaster, N.; Roehl, H. H.; Kimmel, C. B.; Schneider, R.; Hammerschmidt, M. The multidomain protein Brpf1 binds histones and is required for Hox gene expression and segmental identity. *Development* 2008, 135, 1935–1946.

(2) (a) Ullah, M.; Pelletier, N.; Xiao, L.; Zhao, S. P.; Wang, K.; Degerny, C.; Tahmasebi, S.; Cayrou, C.; Doyon, Y.; Goh, S. L.; Champagne, N.; Cote, J.; Yang, X. J. Molecular architecture of quartet MOZ/MORF histone acetyltransferase complexes. *Mol. Cell. Biol.* 2008, 28, 6828–6843. (b) Poplawski, A.; Hu, K.; Lee, W.; Natesan, S.; Peng, D.; Carlson, S.; Shi, X.; Balaz, S.; Markley, J. L.; Glass, K. C. Molecular insights into the recognition of N-terminal histone modifications by the BRPF1 bromodomain. *J. Mol. Biol.* 2014, 426, 1661–1676.

(3) Lubula, M. Y.; Eckenroth, B. E.; Carlson, S.; Poplawski, A.; Chruszcz, M.; Glass, K. C. Structural insights into recognition of acetylated histone ligands by the BRPF1 bromodomain. *FEBS Lett.* 2014, 588, 3844–3854.

(4) Demont, E. H.; Bamborough, P.; Chung, C. W.; Craggs, P. D.; Fallon, D.; Gordon, L. J.; Grandi, P.; Hobbs, C. I.; Hussain, J.; Jones, E. J.; Le Gall, A.; Michon, A. M.; Mitchell, D. J.; Prinjha, R. K.; Roberts, A. D.; Sheppard, R. J.; Watson, R. J. 1,3-Dimethyl Benzimidazolones are potent, selective inhibitors of the BRPF1 bromodomain. *ACS Med. Chem. Lett.* 2014, 5, 1190–1195.

(5) Chung, C. W.; Dean, A. W.; Woolven, J. M.; Bamborough, P. Fragment-based discovery of bromodomain inhibitors part 1: inhibitor binding modes and implications for lead discovery. *J. Med. Chem.* 2012, 55, 576–586.

(6) (a) Hewings, D. S.; Fedorov, O.; Filippakopoulos, P.; Martin, S.; Picaud, S.; Tumber, A.; Wells, C.; Olcina, M. M.; Freeman, K.; Gill, A.; Ritchie, A. J.; Sheppard, D. W.; Russell, A. J.; Hammond, E. M.; Knapp, S.; Brennan, P. E.; Conway, S. J. Optimization of 3,5-dimethylisoxazole derivatives as potent bromodomain ligands. *J. Med. Chem.* 2013, 56, 3217–3227. (b) Zhao, L.; Cao, D.; Chen, T.; Wang, Y.; Miao, Z.; Xu, Y.; Chen, W.; Wang, X.; Li, Y.; Du, Z.; Xiong, B.; Li, J.; Xu, C.; Zhang, N.; He, J.; Shen, J. Fragment-based drug discovery of 2-thiazolidinones as inhibitors of the histone reader BRD4 bromodomain. *J. Med. Chem.* 2013, 56, 3833–3851.

(7) (a) Demont, E. H.; Chung, C. W.; Furze, R. C.; Grandi, P.; Michon, A. M.; Wellaway, C.; Barrett, N.; Bridges, A. M.; Craggs, P. D.; Diallo, H.; Dixon, D. P.; Douault, C.; Emmons, A. J.; Jones, E. J.; Karamshi, B. V.; Locke, K.; Mitchell, D. J.; Mouzon, B. H.; Prinjha, R. K.; Roberts, A. D.; Sheppard, R. J.; Watson, R. J.; Bamborough, P. Fragment-based discovery of low-micromolar ATAD2 bromodomain inhibitors. *J. Med. Chem.* 2015, 58, 5649–5673. (b) Harner, M. J.; Chauder, B. A.; Phan, J.; Fesik, S. W. Fragment-based screening of the bromodomain of ATAD2. *J. Med. Chem.* 2014, 57, 9687–9692.

(8) Ferguson, F. M.; Fedorov, O.; Chaikuad, A.; Philpott, M.; Muniz, J. R.; Felletar, I.; von Delft, F.; Heightman, T.; Knapp, S.; Abell, C.; Ciulli, A. Targeting low-druggability bromodomains: fragment based screening and inhibitor design against the BAZ2B bromodomain. *J. Med. Chem.* 2013, 56, 10183–10187.

(9) Rooney, T. P.; Filippakopoulos, P.; Fedorov, O.; Picaud, S.; Cortopassi, W. A.; Hay, D. A.; Martin, S.; Tumber, A.; Rogers, C. M.; Philpott, M.; Wang, M.; Thompson, A. L.; Heightman, T. D.; Pryde, D. C.; Cook, A.; Paton, R. S.; Muller, S.; Knapp, S.; Brennan, P. E.; Conway, S. J. A series of potent CREBBP bromodomain ligands reveals an induced-fit pocket stabilized by a cation-pi interaction. *Angew. Chem., Int. Ed.* 2014, 53, 6126–6130.

(10) Quinn, E.; Wodicka, L.; Ciceri, P.; Pallares, G.; Pickle, E.; Torrey, A.; Floyd, M.; Hunt, J.; Treiber, D. Abstract 4238: BROMOscan - a high throughput, quantitative ligand binding platform identifies best-in-class bromodomain inhibitors from a screen of mature compounds targeting other protein classes. *Cancer Res.* 2013, 73, 4238.

(11) Philpott, M.; Yang, J.; Tumber, T.; Fedorov, O.; Uttarkar, S.; Filippakopoulos, P.; Picaud, S.; Keates, T.; Felletar, I.; Ciulli, A.; Knapp, S.; Heightman, T. D. Bromodomain-peptide displacement assays for interactome mapping and inhibitor discovery. *Mol. BioSyst.* 2011, 7, 2899–2908.

(12) Hopkins, A. L.; Keseru, G. M.; Leeson, P. D.; Rees, D. C.; Reynolds, C. H. The role of ligand efficiency metrics in drug discovery. *Nat. Rev. Drug Discovery* 2014, 13, 105–121.

(13) Irwin, J. J.; Sterling, T.; Mysinger, M. M.; Bolstad, E. S.; Coleman, R. G. ZINC: a free tool to discover chemistry for biology. *J. Chem. Inf. Model.* 2012, 52, 1757–1768.

(14) (a) Majeux, N.; Scarsi, M.; Apostolakis, J.; Ehrhardt, C.; Caflisch, A. Exhaustive docking of molecular fragments with electrostatic solvation. *Proteins: Struct., Funct., Genet.* 1999, 37, 88–105. (b) Majeux, N.; Scarsi, M.; Caflisch, A. Efficient electrostatic solvation model for protein-fragment docking. *Proteins: Struct., Funct., Genet.* 2001, 42, 256–268.

(15) Unzue, A.; Zhao, H.; Lolli, G.; Dong, J.; Zhu, J.; Zechner, M.; Dolbois, A.; Caflisch, A.; Nevado, C. The "gatekeeper" residue influences the binding mode of acetyl indoles to bromodomains. *J. Med. Chem.* 2016, 59, 3087.

(16) Structural Genomics Consortium (SGC): Bromosporine. http://www.thesgc.org/chemical-probes/bromosporine (accessed January 3, 2016).

(17) Picaud, S.; Strocchia, M.; Terracciano, S.; Lauro, G.; Mendez, J.; Daniels, D. L.; Riccio, R.; Bifulco, G.; Bruno, I.; Filippakopoulos, P. 9H-purine scaffold reveals induced-fit pocket plasticity of the BRD9 bromodomain. *J. Med. Chem.* 2015, 58, 2718–2736.

(18) Magno, A.; Steiner, S.; Caflisch, A. Mechanism and kinetics of acetyl-lysine binding to bromodomains. *J. Chem. Theory Comput.* 2013, 9, 4225–4232.

(19) Zhao, H.; Gartenmann, L.; Dong, J.; Spiliotopoulos, D.; Caflisch, A. Discovery of BRD4 bromodomain inhibitors by fragment-based high-throughput docking. *Bioorg. Med. Chem. Lett.* 2014, 24, 2493–2496.

(20) (a) Xu, M.; Unzue, A.; Dong, J.; Spiliotopoulos, D.; Nevado, C.; Caflisch, A. Discovery of CREBBP bromodomain inhibitors by high-throughput docking and hit optimization guided by molecular dynamics. *J. Med. Chem.* 2016, 59, 1340–1349. (b) Unzue, A.; Xu, M.; Dong, J.; Wiedmer, L.; Spiliotopoulos, D.; Caflisch, A.; Nevado, C.

Fragment-based design of selective nanomolar ligands of the CREBBP bromodomain. *J. Med. Chem.* **2016**, *59*, 1350−1356.

(21) Lolli, G.; Caflisch, A. High-Throughput Fragment Docking into the BAZ2B Bromodomain: Efficient in silico screening for X-ray crystallography. *ACS Chem. Biol.* **2016**, *11*, 800−807.

(22) Kolb, P.; Caflisch, A. Automatic and efficient decomposition of two-dimensional structures of small molecules for fragment-based high-throughput docking. *J. Med. Chem.* **2006**, *49*, 7384−92.

(23) Scarsi, M.; Apostolakis, J.; Caflisch, A. Continuum electrostatic energies of macromolecules in aqueous solutions. *J. Phys. Chem. A* **1997**, *101*, 8098−8106.

(24) (a) MacKerell, A. D.; Bashford, D.; Bellott, M.; Dunbrack, R. L.; Evanseck, J. D.; Field, M. J.; Fischer, S.; Gao, J.; Guo, H.; Ha, S.; Joseph-McCarthy, D.; Kuchnir, L.; Kuczera, K.; Lau, F. T.; Mattos, C.; Michnick, S.; Ngo, T.; Nguyen, D. T.; Prodhom, B.; Reiher, W. E.; Roux, B.; Schlenkrich, M.; Smith, J. C.; Stote, R.; Straub, J.; Watanabe, M.; Wiorkiewicz-Kuczera, J.; Yin, D.; Karplus, M. All-atom empirical potential for molecular modeling and dynamics studies of proteins. *J. Phys. Chem. B* **1998**, *102*, 3586−3616. (b) MacKerell, A. D., Jr.; Feig, M.; Brooks, C. L., 3rd Improved treatment of the protein backbone in empirical force fields. *J. Am. Chem. Soc.* **2004**, *126*, 698−699.

(25) Vanommeslaeghe, K.; Hatcher, E.; Acharya, C.; Kundu, S.; Zhong, S.; Shim, J.; Darian, E.; Guvench, O.; Lopes, P.; Vorobyov, I.; Mackerell, A. D., Jr. CHARMM general force field: A force field for drug-like molecules compatible with the CHARMM all-atom additive biological force fields. *J. Comput. Chem.* **2010**, *31*, 671−690.

(26) Kabsch, W. XDS. *Acta Crystallogr., Sect. D: Biol. Crystallogr.* **2010**, *66*, 125−132.

(27) Evans, P. Scaling and assessment of data quality. *Acta Crystallogr., Sect. D: Biol. Crystallogr.* **2006**, *62*, 72−82.

(28) McCoy, A. J.; Grosse-Kunstleve, R. W.; Adams, P. D.; Winn, M. D.; Storoni, L. C.; Read, R. J. Phaser crystallographic software. *J. Appl. Crystallogr.* **2007**, *40*, 658−674.

(29) Adams, P. D.; Afonine, P. V.; Bunkoczi, G.; Chen, V. B.; Davis, I. W.; Echols, N.; Headd, J. J.; Hung, L. W.; Kapral, G. J.; Grosse-Kunstleve, R. W.; McCoy, A. J.; Moriarty, N. W.; Oeffner, R.; Read, R. J.; Richardson, D. C.; Richardson, J. S.; Terwilliger, T. C.; Zwart, P. H. PHENIX: a comprehensive Python-based system for macromolecular structure solution. *Acta Crystallogr., Sect. D: Biol. Crystallogr.* **2010**, *66*, 213−221.

(30) Emsley, P.; Lohkamp, B.; Scott, W. G.; Cowtan, K. Features and development of Coot. *Acta Crystallogr., Sect. D: Biol. Crystallogr.* **2010**, *66*, 486−501.